Effect of Mg-doping and Fe-doping in lead zirconate titanate (PZT) thin films on electrical reliability

Dongjoo Koh¹, Song Won Ko², Jung In Yang¹, Betul Akkopru-Akgun¹ and Susan Trolier-McKinstry¹

¹Department of Materials Science and Engineering and Materials Research Institute, Pennsylvania State

University

²KOTECH LLC, State College, Pennsylvania, USA

*Corresponding author: Dongjoo Koh / rhehdwn00@gmail.com

Abstract

Uniformly acceptor doped Pb($Zr_{0.48}Ti_{0.52}$)O₃ (PZT) films with 2-mol% Mg or Fe prepared by chemical solution deposition exhibited decreased dielectric constants, and remanent polarizations relative to undoped PZT. For highly accelerated lifetime testing (HALT) at 200°C and an electric field of 300kV/cm in the field up direction, the HALT lifetimes (t₅₀) for undoped, Mg-doped, and Fe-doped PZT films were *shortened* from 2.81 \pm 0.1 hours to 0.21 \pm 0.1, and 0.54 \pm 0.04 hours, respectively. Through thermally stimulated depolarization current (TSDC) measurement, significant $V_0^{\bullet\bullet}$ electromigration was found in homogeneously Mg-doped PZT thin films, a major factor in their short HALT lifetime. Because the concentration of oxygen vacancies increases with uniform acceptor doping, the lifetime decreases. In contrast, when a thin layer of Mg-doped or Fe-doped PZT was deposited on undoped PZT or Nb-doped PZT (PNZT), the HALT lifetimes were *longer* than those of pure PZT or PNZT films. This confirms prior work on PNZT films with a Mn-doped top layer, demonstrating that the HALT lifetime increases for composite films when a layer with multivalent acceptors

is present near the negative electrode during HALT. In that case, the compensating electrons are trapped, presumably on the multivalent acceptors, thus increasing the lifetime.

1. Introduction

Lead zirconate titanate (PZT) thin films are used in microelectromechanical systems (MEMS) as actuators¹, sensors²⁻³, and energy harvesting devices⁴⁻⁵ due to their large piezoelectric coefficients. In order to enable extensive commercial application of these films, combining a high e_{31,f} value and excellent reliability under operating conditions is essential. The electrical reliability of PZT films is strongly influenced by point defect types and concentrations.⁶ Aliovalent impurities in PZT typically lead to predominantly ionic compensation via formation of lead or oxygen vacancies, along with smaller concentrations of electrons or holes.

The lifetime of PZT films under highly accelerated lifetime testing (HALT) conditions is strongly correlated with the electromigration of oxygen vacancies, $V_0^{\bullet\bullet}$. Donor doping of PZT films with higher valence B-site ions like Nb⁵⁺ thus minimizes resistance degradation by lowering the concentration of mobile $V_0^{\bullet\bullet}$.^{7,8} However, acceptor doping PZT with impurities such as Fe^{2+/3+}, Mg²⁺, Mn^{2+/3+} on the B-site (Ti⁴⁺, Zr⁴⁺) generates oxygen vacancies/holes.^{6,9} Under a DC bias electric field, the oxygen vacancies migrate and accumulate near the cathode, leading to electrical degradation of the film.

Recently, however, it was demonstrated that Mn-doped PZT films have *enhanced* lifetimes.^{6,10} The improved resistance degradation in these films was likely due to either¹⁰ (1) Mn-induced Jahn-Teller distortion impeding migration of oxygen vacancies, or (2) electrons preferentially trapping on multivalent Mn, rather than on Ti³⁺. The latter possibility was more consistent with the experimental data.¹⁰

The lifetime of PZT films could be improved still further when a graded doping scheme was utilized, in which a thin Mn-doped PZT layer was added near the cathode of an otherwise Nb-doped film. In some ways, such a graded doping scheme can be envisioned as a simplified version of a multilayer ceramic capacitor (MLCC). Morita et al. In found that Mn-doping in BaTiO3 multilayer ceramic capacitors (MLCC) with Ni-electrode also increased electrical lifetime. In that work, the high concentration of Mn near grain boundaries significantly reduced tunneling currents at a high electrical field and acted as a barrier against oxygen vacancy migration towards the cathode.

The thin film geometry offers the possibility of independently checking the importance of the character of the acceptor used in graded doping, without complications that arise due to changes in the ceramic microstructure. Thus, in this work, the reliability of PZT films with two different types of acceptor doping (i.e. a multivalent acceptor ions without Jahn-Teller distortions ($Fe^{2+/3+/4+}$) and an acceptor with a fixed valence (Mg^{2+}). The effect of uniform vs. graded doping with these acceptors was then assessed.

2. Experimental Procedure

Three sets of PZT films were prepared to study the effects of film composition, film thickness, and graded doping on the HALT lifetime. As shown in Table 1 and Figure 1, the first set of films tested the role of uniform acceptor doping. The second and third set of films was intended to allow the role of graded doping to be assessed.

Figure 1. Schematics of all sample sets (A) 1, (B) 2, and (C) 3.

manuscript. However, the online version of record will be different from this version once it has been copyedited and typeset. PLEASE CITE THIS ARTICLE AS DOI: 10.1063/5.0101308

This is the author's peer reviewed, accepted manuscript. However,

Table 1. Identification of all samples.

Samples		Film composition	Thickness (µm)
Sample set 1	Sample 1-1	Undoped PZT	1.09
	Sample 1-2	Homogeneously Mg-doped PZT	1.08
	Sample 1-3	Homogeneously Fe-doped PZT	0.99
Sample set 2	Sample 2-1	Undoped PZT	1.19
	Sample 2-2	Undoped PZT + Mg-doped PZT top layer	1.16
	Sample 2-3	Undoped PZT + Fe-doped PZT top layer	1.16
Sample set 3	Sample 3-1	PNZT	1.45
	Sample 3-2	PNZT + Mg-doped PZT top layer	1.46
	Sample 3-3	PNZT + Fe-doped PZT top layer	1.44

Solutions of undoped lead zirconate titanate (PbZr_{0.48}Ti_{0.52}O₃), 2-mol% magnesium-doped PZT ((Pb_{0.98}(Zr_{0.48}Ti_{0.52})_{0.98}Mg_{0.02})O₃), and 2-mol% iron-doped lead zirconate titanate ((Pb_{0.98+x}(Zr_{0.48}Ti_{0.52})_{0.98}Fe_{0.02})O₃) films were prepared using chemical solution deposition, where x depends on the oxidation state of the Fe. The solutions had a Zr:Ti ratio of 52:48 and 15% excess lead to reduce the formation of a pyrochlore phase. For Mg and Fe doping, magnesium (II) acetate tetrahydrate and iron (III) nitrate nonahydrate were used. Details on the solution preparation are provided elsewhere. Solutions for the seed layer and the donor doped PZT bulk layer were purchased from Mitsubishi Materials Corporation.

To prepare {001} oriented films, a 2-mol% Nb-doped PZT seed layer was spun on to 6-inch diameter platinized silicon substrates, pyrolyzed at 100°C and 300°C and annealed in a rapid thermal annealer (RTA) at 700°C for 1 minute.

Then, for uniformly acceptor-doped films, the solutions were spin coated at 1500 rpm for 45 seconds on high temperature platinized silicon substrates, and pyrolyzed at 210°C for 2 minutes and 410°C for 2 minutes. The films were annealed in an RTA step at 700°C for 1 minute with 2 slpm O₂ flow and 10°C/sec ramp rate. The process was repeated until a

the online version of record will be different from this version once it has been copyedited and typeset. This is the author's peer reviewed, accepted manuscript. However, the online version of record will be diffe PLEASE CITE THIS ARTICLE AS DOI: 10.1063/5.0101308

thickness of 1 µm was obtained. Undoped films were made using the same thermal treatment steps. For PNZT films, 15 wt% PNZT solutions with 16% Pb excess (Mitsubishi Materials Corporation, Tokyo, Japan) was spin coated on the seed layer at 3000 rpm for 45 seconds and pyrolyzed at 100°C for 1 minute and then at 300°C for 4 minutes. The films were crystallized after every two spin-coated layers with an RTA step at 700°C for 1 minute under O₂ atmosphere.

For samples with graded doping, bulk PZT and PNZT films were prepared as described

above. To minimize the impact of possible processing variations, after PZT or PNZT deposition to the desired layer thickness, the wafer was broken into 3 pieces; one extra 50-70 nm thick layer of undoped PZT, Mg-doped PZT, or Fe-doped PZT solution was added.

For all samples, the top electrodes were patterned through a lift-off process. LOR5A and 3012 photoresist solutions were spin coated on the films at 4500 rpm for 45 seconds and dried at 180°C and 95°C for 1 minute and 3 minutes, respectively. A Karl Suss MABA6 mask aligner was used to expose a pattern of circles with 500 µm diameters. After developing, platinum top electrodes were sputtered on the film using a Kurt J. Lesker CMS-18 tool.

Acetone and CD-26 were used to complete the lift-off. The samples then underwent post-annealing in an RTA at 550°C in air for 1 minute.

The following procedures were used to characterize the resulting films. The frequency and temperature dependent dielectric constant and dielectric loss were measured from 100 Hz to 1 MHz from 50°C to 430°C using an LCR meter (4284A, HP; Hewlett Packard) with a 30 mV AC excitation. Polarization-electric field hysteresis loops were measured at 100 Hz using a Radiant Premier Precision Station (Radiant Technologies, Inc., Albuquerque, New Mexico). The morphology of each film was observed using a field emission scanning electron microscope (FE-SEM, Zeiss Merlin and Gemini 500, Jena, Germany) under an accelerating

voltage of 5 kV. The median lifetime of the films was determined from a highly accelerated life test (HALT) at 200°C and 300kV/cm in the field up direction (that is, the electric field was directed from the bottom to the top electrode). In order to develop adequate statistics, 22 individual electrodes were wire-bonded to a 24-pin DIP package and measured for each HALT run. The thermally stimulated depolarization current (TSDC) was measured for degraded, undoped, and homogeneously Mg- or Fe-doped PZT thin films with respect to various poling fields (field up direction) and heating rates. Activation energies for each TSDC peak were calculated based on the heating rate method.

3. Results and Discussion

3.1 Thin Film Microstructures

Figure 2 shows the microstructures of the different types of film. Calculations of average grain size were based on a line intercept method using ImageJ. Three different SEM surface micrographs were used for the calculations for each sample type. For sample set 1, the grain size varied from 40 nm to 250 nm. The differences in grain size are presumably a function of a non-uniform distribution of nucleation sites. The average grain size of all samples is shown in supplementary Table 1. It is notable that the grain sizes for all samples fall within error bounds of each other. Although other researchers have reported that niobium doping either increases ^{12,13} or decreases ^{14,15} the PZT grain size, no such effect was seen here.

Pyrochlore (or fluorite) grains are also detected near the grain boundaries, as is widely reported in PZT films with slightly lead deficient surfaces. ^{16,17} The surface pyrochlore seen for samples 2-2 and 3-2 was relatively modest, and strong {100} crystallographic orientation of the perovskite phase was retained. This, combined with the comparable dielectric

properties relative to other samples suggests that the pyrochlore phase does not lead to a significant change in the response of the films.

Figure 2. FE-SEM images of microstructure of all film samples. The larger grains shown are perovskite PZT, while the very small lighter colored spots near the grain boundaries are from a pyrochlore or fluorite phase.

3.2 Baseline Properties

As shown in the supplementary Table 2, all of the films had relative permittivities of ~1100 – 1500, with loss tangents <3%. Acceptor doping slightly reduced the relative permittivity for Fe-doped films; the relative permittivity of Mg doped films was higher. This may be due, at least in part, to a lower Curie temperature, as described in the supplementary Table 3.

Figure 3. P-E hysteresis loops of all films from (A) Sample set 1, (B) Sample set 2, (C) Sample set 3

Figure 3 shows polarization – electric field hysteresis loops for all samples. Figure 3A shows that the remanent polarization (P_r) and coercive field (E_c) of samples 1-1, 1-2, and 1-3 measured at a maximum field of 400 kV/cm were about 17 ± 0.2 , 15 ± 0.2 , and 16 ± 0.3 μ C/cm² and 29 ± 0.2 , 30 ± 0.2 , 30 ± 0.2 kV/cm. Presumably, the lower P_r values of samples 1-2 and 1-3 compared to 1-1 can be attributed to acceptor-doping. For acceptor-doped PZT there is the possibility that defects may be prone to association, e.g., $Mg_{Ti}^{"}$ - $V_0^{\bullet \bullet}$ or $Fe_{Ti}^{'}$ - $V_0^{\bullet \bullet}$, producing local electric and strain fields. Consequently, they act as pinning centers and reduce the irreversible domain wall motion. Zhu et al. ¹⁸ reported that Mn-doped PZT films exhibited lower domain wall motion compared to undoped PZT films for this reason. All

films in sample set 2 exhibited similar P_r and E_c values of about 16 ± 0.2 , 15 ± 0.2 , and 16 ± 0.3 $\mu\text{C/cm}^2$ and 30 ± 0.2 , 30 ± 0.2 , 30 ± 0.2 kV/cm, measured at a maximum electric field of 400 kV/cm. For sample set 3, higher remanent polarization and lower coercive energy values were found compared to those in sets 1 and 2. P_r and E_c of samples 3-1, 3-2, and 3-3 measured at 400 kV/cm were about 21 ± 0.3 , 21 ± 0.3 , and 21 ± 0.5 $\mu\text{C/cm}^2$ and 27 ± 0.2 , 27 ± 0.2 , and 27 ± 0.2 kV/cm, respectively. The differences could be due to donor-doped bulk films (PNZT) as these films contain lower oxygen vacancy concentrations.

3.3 Highly Accelerated Lifetime Test (HALT)

To investigate the effects of Mg²⁺ and Fe^{2+/3+} acceptor doping in PZT thin films on reliability, HALT measurements were performed on sample set 1 (Figure 4) at 200°C and 300 kV/cm. An electric field was applied in the field up direction, in which positive voltage was applied to the bottom electrode and the top electrodes were grounded. The median lifetime (t₅₀) was determined from the time when half of the samples electrically failed. The time at which the leakage current density exceeded the minimum leakage by two orders of magnitude was considered to be the failure time.

It was found that homogeneously acceptor doped PZT samples have shorter t_{50} than pure PZT; 2.84 ± 0.30 , 0.21 ± 0.04 , 0.54 ± 0.03 hours for sample 1-1, 1-2, and 1-3, respectively. This was attributed to the higher oxygen vacancy concentration throughout the acceptor doped PZT films. That is, replacement of Ti^{4+} sites with lower valence ions (Mg²⁺ and Fe^{2+/3+/4+}) generates more $V_0^{\bullet\bullet}$ for charge compensation. Oxygen vacancies electromigrate towards the cathode during electrical degradation. Thus, it is reasonable that degradation was exacerbated by higher oxygen vacancy concentration induced by acceptor doping. It is also notable that the lifetime of the Fe-doped sample exceeds that of the Mg doped sample for the

same doping concentration, presumably because of a higher $V_0^{\bullet\bullet}$ concentration in the Mg-doped sample.

Figure 4. Median lifetime (t₅₀) of (A) sample set 1, (C) sample set 2, and (E) sample set 3 and variation in leakage current density with time in (B) sample set 1, (D) sample set 2, and (F) sample set 3.

Sample sets 2 and 3 also underwent HALT measurements under the same conditions (200°C and 300 kV/cm). The electric field was applied in the field up direction, such that the acceptor doped layer was located on the cathode side. Several points are apparent from the data. First, comparing samples 1-1 and 2-1, a longer lifetime is observed for the thicker undoped PZT film. This is unsurprising, because the leakage current starts to rise one enough $V_0^{\bullet\bullet}$ have electromigrated to the dielectric/electrode interface to lower the Schottky barrier height. Secondly, the electrical conductivity rises with acceptor doping, and falls with donor doping, consistent with partial electronic compensation of the dopants in p-type films. Third, the lifetimes are substantially larger for the thicker Nb-doped bulk layers in the film, as expected by the combination of a longer migration distance and smaller concentration of oxygen vacancies.

Fourth, it was observed that samples with graded doping (sample sets 2 and 3) have a *longer* lifetime than either undoped PZT and PNZT films (sample 2-1 and 3-1). The measured t_{50} was 4.7 ± 0.3 , 6.8 ± 0.8 , and 8.2 ± 1.3 hours for samples 2-1, 2-2, and 2-3, respectively. In the same way, t_{50} was 15.9 ± 1.0 , 16.6 ± 1.6 , and 17.9 ± 2.1 hours for samples 3-1, 3-2, and 3-3, respectively.

3.4 Thermally Stimulated Depolarization Current (TSDC) Measurements

To investigate the types of defects leading to resistance degradation of the PZT thin films, thermally stimulated depolarization current (TSDC) measurements were performed on electrically degraded films from sample set 1. Samples were degraded under a DC poling field at elevated temperature and cooled down under the field to freeze defects into a poled state. The depolarization current was then measured while re-heating at a constant ramp rate under zero bias.

As reported elsewhere, the temperature at which a maximum is observed in the TSDC

As reported elsewhere, the temperature at which a maximum is observed in the TSDC current, T_{max}, shifts in different directions with respect to the poling field depending on the physical origin of the current.^{6,19,20} When T_{max} increases with increased poling field, the depolarization current results from space charge.^{6,19,20} (In PZT thin films, defect dipoles can be dissociated under electric fields and the oxygen vacancies then undergo electromigration. As this occurs, the local internal field associated with the original defect dipoles is replaced by an average electric field across the films.) When T_{max} remains the same with increased poling field, the TSDC peak is attributed to defect dipoles. When T_{max} decreases with increased poling field, the TSDC peak is attributed to trapped charges.^{6,19,20} In this study, the heating rate method was chosen to evaluate the activation energies ^{6,19,20,21} using heating rates of 2, 6 and 10°C/minute. For each TSDC curve, T_{max} of the peak was determined via curve fitting; the results are reported in Table 2.

Three different peaks were observed in the undoped PZT films (sample 1-1), as shown in Figure 5A. The peak cleaning method (removal of peaks at lower temperatures than the desired peaks) was used to identify peak 3. Based on the shift in T_{max} with increasing poling field, the physical origin of the three peaks were speculated to be trapped charge, trapped charge, and space charge, respectively. The calculated activation energies for peaks 1-3 were 1.14 ± 0.02 eV, 1.20 ± 0.14 eV, and 0.51 ± 0.09 eV, respectively. The activation energies in peaks 1 and 2 are consistent with electron trapping by $Ti^{3+/4+}$, as reported in the literature. It

is possible that the two trapped charge induced peaks were caused by different electron trapping sites, potentially within individual crystallization layers and between layers. Typical sol-gel based PZT thin films form a Zr/Ti compositional gradient within each crystallized layer.²² The bottom of each layer is Ti-rich; the top of each layer is Zr-rich. This gradient can, in principle, produce two different ranges for trap-to-trap emissions and lead to two trapped charge induced peaks, as observed in this study. The activation energy calculated for the third peak is close to that reported for space charge by migration of oxygen vacancies.^{6,23}

Figure 5. TSDC data for (A, B) sample 1-1, (C, D) sample 1-2, and (E, F) sample 1-3. For A, C, and E, poling was conducted at 180°C for 4 hours and the TSDC data were measured using a ramp rate of 10°C/min. For B, D, and F, the TSDC measured at ramp rates of 2, 6, 10°C/min after poling at 200 kV/cm at 180°C for 4 hours.

The TSDC results for homogeneously Mg-doped PZT thin films (sample 1-2) are shown in Figure 5C. Peak 1 was from trapped charges, as indicated by a decrease in T_{max} with increased poling field. Peak 2 is believed to result from space charge induced by migration of oxygen vacancies, given that T_{max} increased with increasing poling field. However, the activation energy of the peak was calculated to be 1.03 ± 0.03 eV, approximately two times higher than the value reported in the literature (~ 0.6 eV). $^{6.23}$ This value is closer to the activation energy of a space charge induced by the short-range migration of oxygen vacancies (~ 1.1 eV) for Mg-doped BaTiO₃ bulk ceramics, as reported by Yoon et al. 24 In that work, oxygen vacancy migration was blocked by grain boundaries and formed a $V_0^{\bullet \bullet}$ concentration gradient within grains of the bulk ceramic due to low $V_0^{\bullet \bullet}$ diffusion rates at the grain boundaries.

The $V_0^{\bullet\bullet}$ migration blocking effect, however, has not been reported in lead zirconate titanate thin films. Grain boundaries form parallel to the film thicknesses and create columnar structures in oriented PZT films, thus grain boundaries are unlikely to be the source of local $V_0^{\bullet\bullet}$ migration barriers. It is possible however, that a blocking effect exists layer by layer

Figure 6. Schematic of gradient in oxygen vacancy concentration in sample 1-2 after poling.

characteristic of sol-gel PZT in each layer might lower the $V_0^{\bullet \bullet}$ diffusion rate. 12,22,25

instead of grain by grain in PZT films (Figure 6). That is, the Zr/Ti compositional gradient

The space charge peak in sample 1-2 implies that high concentrations of oxygen vacancies were present due to the Mg-doping. Moreover, this sample shows much higher magnitudes of the TSDC peaks than the other samples, suggesting a higher defect density (oxygen vacancy or/and trapped charge concentration). It is unlikely that the difference is associated with differences in the pyroelectric response alone, since Tc is similar for the three films. A higher oxygen vacancy concentration accumulated near the cathode can cause severe band bending, which in turn enhances the charge injection and subsequent electron trapping by Ti⁴⁺. These findings are consistent with HALT results. Higher defect concentrations lead to lower lifetime; the mean time to failure (MTTF) decreases in the same order as the magnitude of the TSDC peaks.

As shown in Figure 5E, two TSDC peaks were detected at 160° C and 250° C in sample 1-3. For both peaks, T_{max} decreased with increased poling fields, indicating trapped charge. The activation energy for peak 1 was 0.90 ± 0.12 eV. This value is slightly lower than the activation energy for electron trapping by $Ti^{3+/4+}$ ions, as reported in other studies (~1.1 eV). The activation energy for peak 2 was 1.12 ± 0.02 eV, in good agreement with electron trapping by $Ti^{3+/4+}$ ions. ^{6,23} The origin of the two trapped charge peaks is expected to be comparable to those of the undoped films (sample 1-1).

This is the author's peer reviewed, accepted manuscript. However, the online version of record will be different from this version once it has been copyedited and typeset. PLEASE CITE THIS ARTICLE AS DOI: 10.1063/5.0101308

Table 2. Activation energies of TSDC peaks for sample 1-1, 1-2, and 1-3.

	Peak	E _a (eV)	Physical origin
Sample 1-1	1	1.14 ± 0.02	Interlayer Electron trapping by Ti ^{3+/4+} ions
	2	1.20 ± 0.14	Intralayer Electron trapping by Ti ^{3+/4+} ions
	3	0.51 ± 0.09	Space charge by Vo migration
Sample 1-2	1	-	Electron trapping by Ti ^{3+/4+} ions
	2	1.03 ± 0.03	Space charge by short-range V ₀ migration
Sample 1-3	1	0.90 ± 0.12	Interlayer Electron trapping by Ti ^{3+/4+} ions
	2	1.12 ± 0.02	Intralayer Electron trapping by Ti ^{3+/4+} ions

It is interesting to consider the HALT data for the films with graded doping in light of the TSDC data. As shown above, the HALT lifetime is higher for films with an acceptor doped layer near the cathode than for a homogeneously doped film of the same thickness. These results run counter to the observations on homogeneous films. If the dominant factor for lifetime was the concentration of oxygen vacancies, then the addition of an acceptor doped PZT top layer to either PZT or PNZT films would yield a *lower*, rather than a *higher* HALT lifetime.

3.5 Comparison with Multilayer Ceramic Capacitors (MLCC)

The films with graded doping used in this work can be seen as a two-dimensional analog of a core-shell multilayer ceramic capacitor (MLCC). Chazono and Kishi have demonstrated that the shell layer provides an additional barrier to the migration of oxygen vacancies, and so increased the lifetime. Manganese doping also produced in increase in lifetime, which was reported to be due to a reduction in the mobility of the oxygen vacancies. Morita et al. amplified this model, demonstrating that improved fits to the impedance data were obtained when it was presumed that electron trapping occurs in the shell layer. The data for the PZT films in this work are analogous to these prior reports in that the acceptor layer near the

the online version of record will be different from this version once it has been copyedited and typeset.

This is the author's peer reviewed, accepted manuscript. However, the online version of record will be diffe PLEASE CITE THIS ARTICLE AS DOI: 10.1063/5.0101308 cathode provides an additional barrier for the lowering of the Schottky barrier that governs conduction.

There are, however, a few differences between the behavior of MLCC and thin PZT films. First, it is noted that in no case was evidence found for a tunneling current analogous to those reported in MLCC ceramics with core-shell microstructures.²⁷ Instead, in the films, the change in the interface at which electrons would be injected acts as the second barrier to failure. For example, the Mg-doped PZT layer would be more p-type and the region near the Pt electrode would be more n-type as a result of the electrode deposition processes. This could induce an additional barrier for electron transport in the surface layer. It is also possible that Mg-doping widened the band gap of PZT due to higher ionicity, which would slightly change the Schottky barrier height.²⁸ Second, as seen in this paper, PZT films uniformly doped with Mg and Fe have very short lifetimes due to the higher concentration of oxygen vacancies. That is, the short HALT lifetimes of uniformly Mg- or Fe-doped layers do not appear to act as barriers for migration of oxygen vacancies, as was the case for the core-shell MLCC. Third, the defect chemistry near the dielectric/electrode interface governs the electrical degradation in PZT films. A strong voltage polarity dependent electrical reliability characteristic was observed in PZT films due to variation in (1) oxygen vacancy distribution, (2) valence state of redox active acceptor ions, and (3) Ti/Zr segregation. ^{6,12,22,25} Finally, it should be noted that Fe is a multivalent ion and acts as an electron trap site. It is notable that for both PZT and PNZT films, the Fe-doped top layer produces a higher lifetime than the Mg-doped top layer, suggesting that multivalent acceptors may be useful in increasing lifetime relative to acceptors with fixed charge. Trapped electrons would need to hop between the low concentration of Fe ions (electron trap sites) to enable conductivity. This spreads out the width of the layer providing charge compensation for the oxygen

the online version of record will be different from this version once it has been copyedited and typeset.

This is the author's peer reviewed, accepted manuscript. However, the online version of record will be diffe PLEASE CITE THIS ARTICLE AS DOI: 10.1063/5.0101308 vacancies, and makes it more difficult to decrease the Schottky barrier height for electron injection, as described elsewhere.^{6,10}

It should be noted that the electrical conductivity of the Mg-doped material is higher than that of either the Fe-doped or the undoped PZT. Thus, the increase in HALT lifetime for films with graded doping is not due only to the addition of a higher conductivity layer reducing the mobility of oxygen vacancies by shunting the field. Instead, the multivalent character of the acceptor is important, as was previously shown for films with graded doping when Mn was used as the multivalent ion.¹⁰

From the standpoint of property changes, it is known that for piezoelectric bulk ceramics, the migration of oxygen vacancies on poling, space charge, as well as the alignment of defect dipoles can act to stabilize the polarization state on poling, and so can reduce the extrinsic contributions to the piezoelectric response. In thin films, imprint developed during poling or degradation can also act to stabilize the domain state, with improved long-term stabilization occurring for acceptor-doped films in which oxygen vacancy migration dominates the imprint, relative to acceptor-doped films for which charge injection from the electrodes dominates imprint.³⁰ In both cases, the internal bias acted to increase the small signal piezoelectric coefficient. The large signal response was decreased as substantive poling contributions were eliminated, but at the expense of additional hysteresis and self-heating.³¹

4. Conclusions

In this work, the nature of the acceptor dopant in PZT thin films with graded doping was investigated. HALT measurements were performed for all samples under 300 kV/cm at 200°C. The lifetime of undoped PZT was found to be longer compared to homogeneously Mg and Fe-doped PZT films. However, undoped PZT and PNZT had shorter lifetimes than films

with a top layer of the acceptor doped PZT for degradation in the field up direction.

Migration and accumulation of oxygen vacancies towards the cathode was the underlying mechanism that drove failure. It was found that multilayer donor/acceptor doped structures are useful in increasing the lifetime of PZT films. However, the character of the acceptor matters. The lifetime increased less when the acceptor-doped layers utilized Mg, which has a single, well-defined valence state. High degree of oxygen vacancy migration was detected in

homogeneously Mg-doped PZT thin films through thermally stimulated depolarization

provides a significantly higher lifetime than either Mg or Fe doping in the top layer.

current measurement. The lifetime increases when Fe is used as an acceptor. However, Mn

Supplementary Material

See the supplementary material for temperature dependent dielectric constant and dielectric loss of sample set 1 (Figure S1), XRD patterns of all samples (Figure S2), average grain size of all samples (Table S1), average dielectric constant and dielectric loss of all samples (Table S2), and Curie temperature measured for sample set 1 (Table S3).

Acknowledgements

The authors gratefully acknowledge partial financial support from the Center for Dielectrics and Piezoelectrics and the National Science Foundation under Grant Nos. IIP-1361571 and IIP-1841453. Kim Trolier is thanked for her help in editing the manuscript.

Author Declarations

Conflict of Interest

The authors have no conflicts to disclose.

Data Availability

The data that support the findings of this study are available from the corresponding author upon reasonable request.

the online version of record will be different from this version once it has been copyedited and typeset.

This is the author's peer reviewed, accepted manuscript. However, the online version of record will be diffe PLEASE CITE THIS ARTICLE AS DOI: 10.1063/5.0101308

References

- H. Kueppers, T. Leuerer, U. Schnakenberg, W. Mokwa, M. Hoffmann, T. Schneller, U. Boettger, R. Waser, "PZT thin films for piezoelectric microactuator applications," Sensors and Actuators. A., 97-8, 680-684 (2002). https://doi.org/10.1016/S0924-4247(01)00850-0
- G. L. Smith, J. S. Pulskamp, L. M. Sanchez, D. M. Potrepka, R. M. Proie, T. G. Ivanov, R. Q. Rudy, W. D. Nothwang, S. S. Bedair, C. D. Meyer, and R. G. Polcawich, "PZT-based piezoelectric MEMS technology," Journal of the American Ceramic Society, 95[6], 1777-1792 (2012). https://doi.org/10.1111/j.1551-2916.2012.05155.x
- P. Muralt, R. G. Polcawich, and S. Trolier-McKinstry, "Piezoelectric thin films for sensors, actuators, and energy harvesting," MRS Bulletin, 34[9], 658-664 (2009). https://doi.org/10.1557/mrs2009.177
- 4. H. G. Yeo, X. Ma, C. Rahn and S. Trolier-McKinstry, "Efficient piezoelectric energy harvesting utilizing (001) textured bimorph PZT films on flexible metal foils," Advanced Functional Materials, 26[32], 5040-5046 (2016). https://doi.org/10.1002/adfm.201601347
- K. Morimoto, I. Kanno, K. Wasa, and H. Kotera, "High-efficiency piezoelectric energy harvestors of c-axis-oriented epitaxial PZT films transferred onto stainless steel cantilevers," Sensors and Actuators, 163[1], 428-432 (2010). https://doi.org/10.1016/j.sna.2010.06.028
- 6. B. Akkopru-Akgun, T. Bayer, K. Tsuji, C. A. Randall, M.T. Lanagan, and S. Trolier-McKinstry, "The influence of Mn doping on the leakage current mechanisms and resistance degradation behavior in lead zirconate titanate films," Acta Materialia, 208, 116680 (2021). https://doi.org/10.1016/j.actamat.2021.116680

- This is the author's peer reviewed, accepted manuscript. However, the online version of record will be different from this version once it has been copyedited and typeset. PLEASE CITE THIS ARTICLE AS DOI: 10.1063/5.0101308
- 7. J. H. Park, B. K. Kim, K. H. Song, and S. J. Park, "Piezoelectric properties of Nb₂O₅ co-doped Pb(Zr_{0.53}Ti_{0.47})O₃ ceramics," Journal of Materials Science: Materials in Electronics, 6, 97-101 (1995). https://doi.org/10.1007/BF00188191
- 8. J-S. Yang, Y. S. Kang, I. Kang, S. M. Lim, S-J. Shin, J. W. Lee, and K. H. Hur, "Comparison of the thermal degradation of heavily Nb-doped and normal PZT thin films," IEEE UFFC, 64[3], 617-622 (2017). https://doi.org/10.1109/tuffc.2017.2647971
- C. Slouka, T. Kainz, E. Navickas, G. Walch, H. Hutter, K. Reichmann, and J. Fleig, "Effect of acceptor and donor doping on oxygen vacancy concentrations in lead zirconate titanate (PZT)," Materials, 9[11], 945 (2016). http://dx.doi.org/10.3390/ma9110945
- 10. W. Zhu, B. Akkopru-Akgun, J. Yang, C. Fragkiadakis, K. Wang, S. Ko, P. Mardilovich, and S. Trolier-McKinstry, "Influence of graded doping on the long-term reliability of Nb-doped lead zirconate titanate films", Acta Materialia, 12[9], 117251 (2021). https://doi.org/10.1016/j.actamat.2021.117251
- 11. K. Morita, Y. Mizuno, H. Chazono, and H. Kishi "Effect of Mn addition on deelectrical degradation of multilayer ceramic capacitor with Ni internal electrode," The Japan Society of Applied Physics, 41, 6957 (2002). https://doi.org/10.1143/JJAP.41.6957
- 12. T. M. Borman, "{001} textured growth of doped, gradient free, lead zirconate titanate thin films by chemical solution deposition," M.S. thesis, The Pennsylvania State University; 2016. 178 p.
- 13. T. Haccarat, D. Remiens, & E. Cattan, "Substitution of Nb doping on the structural, microstructural and electrical properties in PZT films," Thin Solid Films, 423, 235-242 (2003). http://dx.doi.org/10.1016/S0040-6090(02)01045-3

- This is the author's peer reviewed, accepted manuscript. However, the online version of record will be different from this version once it has been copyedited and typeset. PLEASE CITE THIS ARTICLE AS DOI: 10.1063/5.0101308
- 14. M. Pereira, A. G. Peixoto, and M. J. M. Gomes, "Effect of Nb doping on the microstructural and electrical properties of the PZT ceramics," Journal of the European Ceramic Society, 21[10], 1353-1356 (2001).
 http://dx.doi.org/10.1016/S0955-2219(01)00017-6
- 15. M. D. Durruthy, L. Fuentes, M. Hernandez, and H. Camacho, "Influence of the niobium dopant concentration on the Pb(Zr_{0.54}Ti_{0.46})O₃ ceramic sintering and final properties," Journal of Materials Science, 35[9], 2311-2317 (2000). http://dx.doi.org/10.1023/A:1004751632634
- 16. S. A. Kukushkin, I. Y. Tentilova, and I. P. Pronin, "Mechanism of the phase transformation of the pyrochlore phase into the perovskite phase in lead zirconate titanate films on silicon substrates," Physics of Solid State, 54[3], 611-616 (2012). http://dx.doi.org/10.1134/S1063783412030158
- 17. N. Mukhin, D. Chigirev, L. Bakhchova, and A. Tumarkin, "Microstructure and properties of PZT films with different PbO content ionic mechanism of built-in fields formation," Materials, 12[18], 2926 (2019). https://doi.org/10.3390/ma12182926
- 18. W. Zhu, I. Fujii, W. Ren, & S. Trolier-McKinstry, "Influence of Mn doping on domain wall motion in Pb(Zr_{0.52}Ti_{0.48})O₃ films," Journal of Applied Physics, 109[6], 064105 (2011). https://doi.org/10.1063/1.3552298
- 19. W. Liu, and C. A. Randall, "Thermally stimulated relaxation in Fe-doped SrTiO₃ systems: I. single crystals," Journal of American Ceramic Society, 91[10], 3245-3250 (2008). https://doi.org/10.1111/j.1551-2916.2008.02595.x
- 20. W. Liu, and C. A. Randall, "Thermally stimulated relaxation in Fe-doped SrTiO₃ systems: II. Degradation of SrTiO₃ dielectrics," Journal of American Ceramic Society, 91[10], 3251-3257 (2008). https://doi.org/10.1111/j.1551-2916.2008.02613.x

- This is the author's peer reviewed, accepted manuscript. However, the online version of record will be different from this version once it has been copyedited and typeset.

 PLEASE CITE THIS ARTICLE AS DOI: 10.1063/5.0101308
- 21. R-V. Wang, P. C. McIntyre, "¹⁸O tracer diffusion in PbZrTiO₃ thin films: A probe of local oxygen vacancy concentration," Journal of Applied Physics, 97, 023508-1-8 (2005). https://doi.org/10.1063/1.1814813
- 22. F. Calame and P. Muralt, "Growth and properties of gradient free sol-gel lead zirconate titanate thin films," Applied Physics Letters, 90, 062907 (2007). https://doi.org/10.1063/1.2472529
- 23. M.V. Raymond, and D. M. Smyth, "Defects and charge transport in perovskite ferroelectrics," Journal of Physics and Chemistry of Solids, 57: 1507-1511 (1996). https://doi.org/10.1016/0022-3697(96)00020-0
- 24. S-H. Yoon, C. A. Randall, and K-H. Hur, "Correlation between resistance degradation and thermally stimulated depolarization current in Acceptor (Mg)-doped BaTiO₃ submicrometer fine-grain ceramics," Journal of American Ceramic Society, 93[7] 1950-1956 (2010). https://doi.org/10.1111/j.1551-2916.2010.03647.x
- 25. S. Pelloquin, G. Le Rhun, E. Defaÿ, P. Renaux, E. Nolot, J. Abergel, and H. Sibuet, "Improvement of Capacitive Behavior on Gradient-Free PZT Thin Films," Integrated Ferroelectrics 157, 132–138 (2014). https://doi.org/10.1080/10584587.2014.912887
- 26. H. Chazono and H. Kishi, "DC-electrical degradation of the BT-based material for multilayer ceramic capacitor with Ni internal electrode: impedance analysis and microsctructure," The Japan Society of Applied Physics, 40, 5624 (2001). https://doi.org/10.1143/JJAP.40.5624
- 27. K. Morita, Y. Mizuno, H. Chazono, H. Kishi, G. Y. Yang, W. E. Liu, E. C. Dickey, and C. A. Randall, "Electric conduction of thin-layer Ni-multilayer ceramic capacitors with core-shell structure BaTiO₃," The Japan Society of Applied Physics, 46, 2984 (2007). https://doi.org/10.1143/JJAP.46.2984

- 28. S. Trolier-McKinstry and R. E. Newnham, "Material engineering: bonding, structure, and structure-property relationships," Cambridge University Press, (2017). https://doi.org/10.1557/mrs.2019.147
 29. B. Akkopru-Akgun, W. Zhu, C. A. Randall, M. T. Lanagan, and S. Trolier-
- 29. B. Akkopru-Akgun, W. Zhu, C. A. Randall, M. T. Lanagan, and S. Trolier-McKinstry, "Polarity dependent DC resistance degradation and electrical breakdown in Nb doped PZT films," APL Materials, 7, 120901 (2019). https://doi.org/10.1063/1.5115391
- 30. B. Akkopru-Akgun, W. Zhu, M. T. Lanagan, and S. Trolier-McKinstry, "The effect of imprint on remanent piezoelectric properties and ferroelectric aging of PbZr_{0.52}Ti_{0.48}O₃ thin films," Journal of the American Ceramic Society, 102[9] 5328-5341 (2019). https://doi.org/10.1111/jace.16367
- 31. J. S. Lundh, W. Zhu, Y. Song, S. W. Ko, C. Fragkiadakis, P. Mardilovich, S. Trolier-McKinstry, and S. Choi, "Local measurements of domain wall-induced self-heating in released PbZr_{0.52}Ti_{0.48}O₃ films," Journal of Applied Physics, 128[21] 214102 (2020). https://doi.org/10.1063/5.0029582

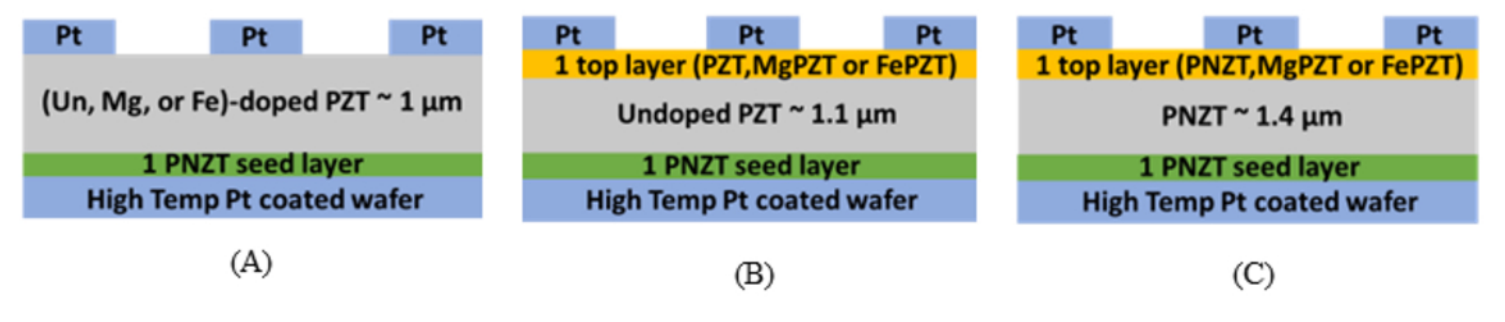


Figure 1. Schematics of all sample sets (A) 1, (B) 2, and (C) 3.

Undoped PZT (1-1) Mg-doped PZT (1-2) Fe-doped PZT (1-3) 200 nm 200 nm 200 nm 209 ± 39 nm 231 ± 53 nm 223 ± 34 nm Undoped PZT (2-1) PZT + Mg-doped PZT PZT + Fe-doped PZT (2-2)(2-3)200 nm 200 nm 200 nm 190 ± 31 nm 209 ± 33 nm 239 ± 25 nm Nb-doped PZT (3-1) PNZT + Mg-doped PZT PNZT + Fe-doped PZT (3-2)(3-3)200 nm 200 nm 200 nm 210 ± 29 nm 228 ± 39 nm 242 ± 45 nm

Figure 2. FE-SEM images of microstructure of all film samples. The larger grains shown are perovskite PZT, while the very small lighter colored spots near the grain boundaries are from a pyrochlore or fluorite phase.

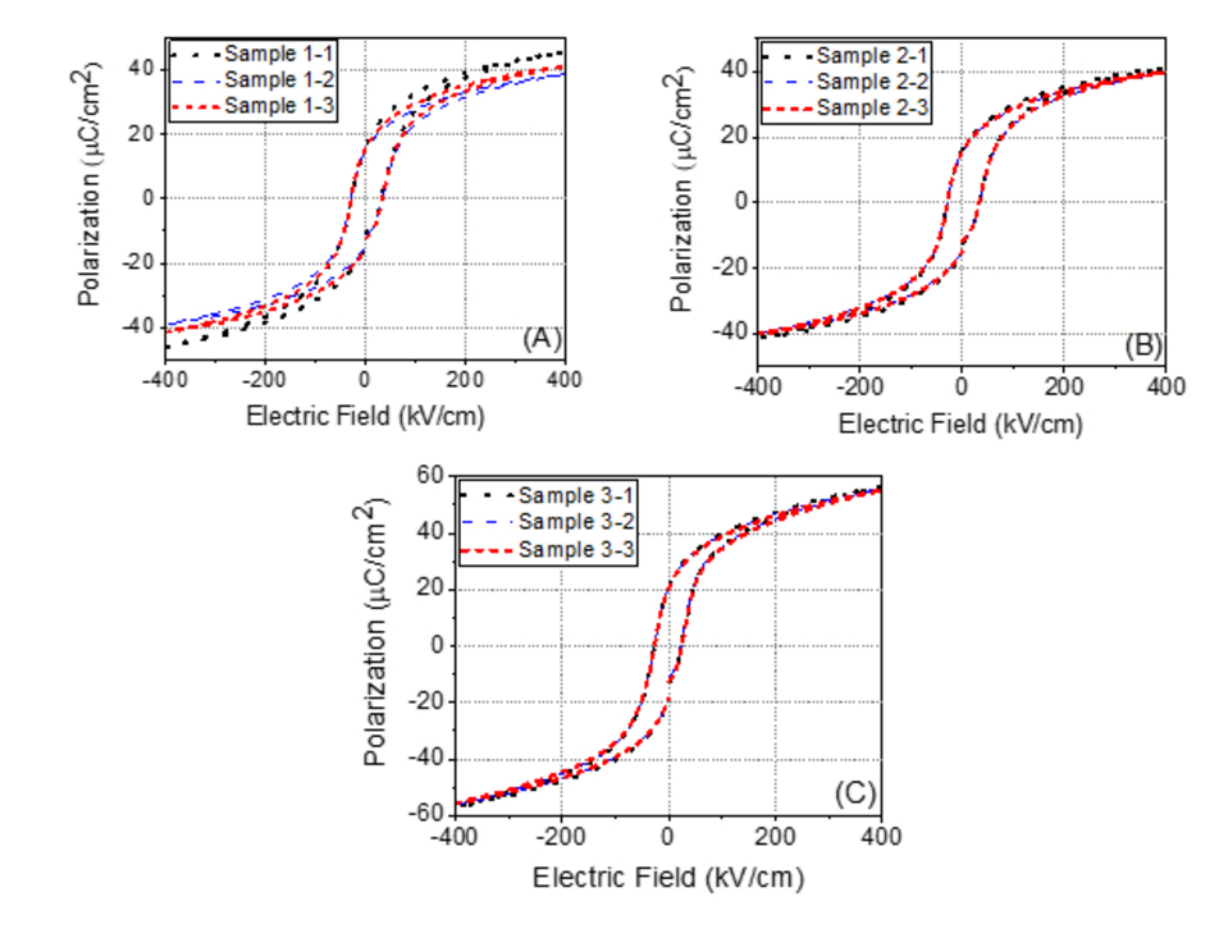


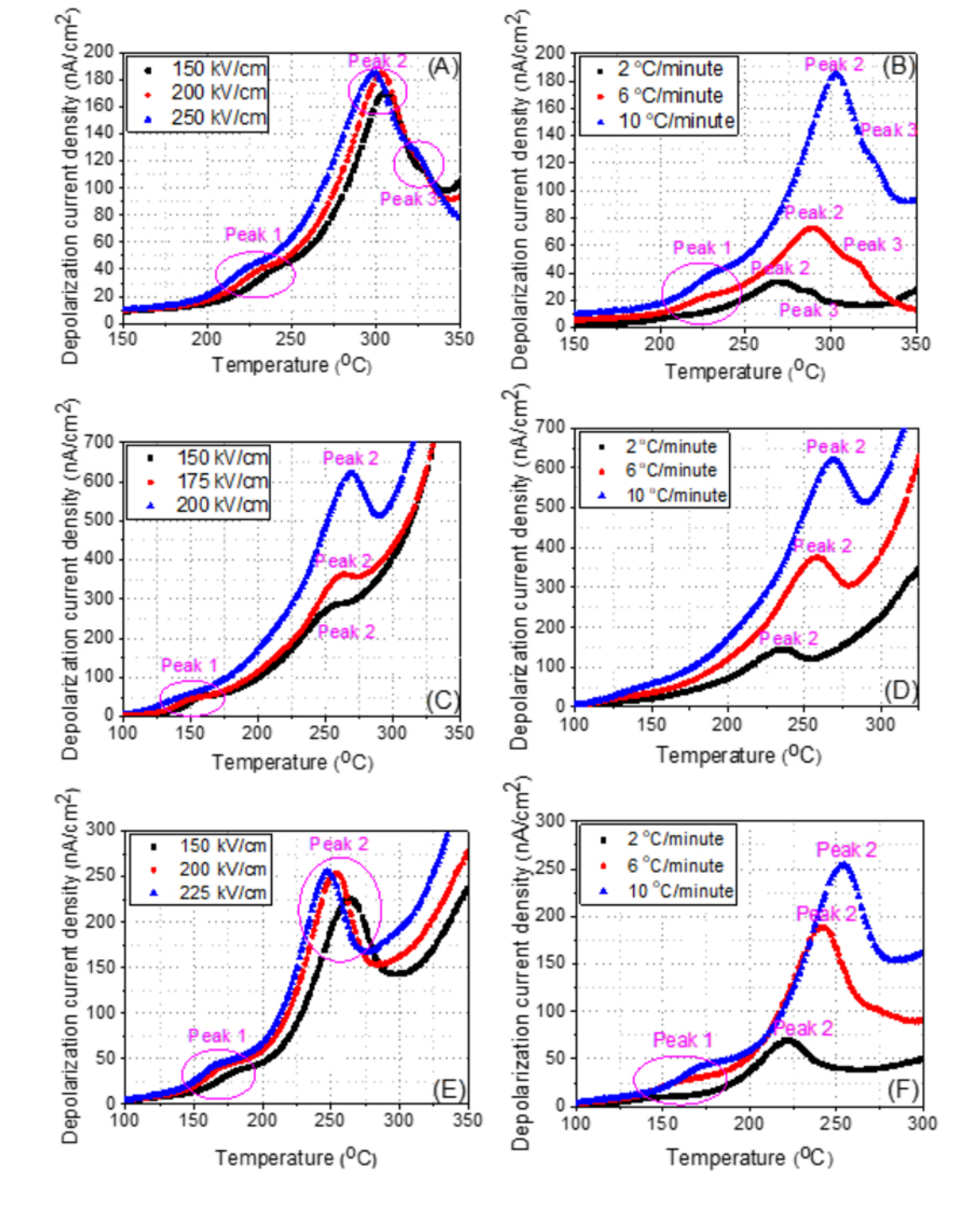
Figure 3. P-E hysteresis loops of all films from (A) Sample set 1, (B) Sample set 2, (C) Sample set 3

Leakage Current Density (A/cm²) --- Sample 1-1 --- Sample 1-2 99.999 Sample 1-3 Sample 1-1 (t₅₀ ~ 2.84 hr) Sample 1-2 (t50 ~ 0.21 hr Probability (%) 99.5 Sample 1-3 (t50 ~ 0.54 hr 0.01 0.001 70 1E-4 (B) 1E-5 100 1000 10 10000 100000 100 1000 10000 Time to Failure (second) Time (second) --Sample 2-1 99.999 Sample 2-2 Sample 2-1 (t₅₀ ~ 4.70 hr) Probability (%) Sample 2-3 Sample 2-2 (t₅₀ ~ 6.81 hr) 99.5 Sample 2-3 (t50 ~ 8.21 hr) 70 10 (D) 1000 100000 10000 10000 100000 Time to Failure (second) e Current Density (A/cm²) L Time (second) - Sample 3-1 99.999 Sample 3-2 Sample 3-1 (t₅₀ ~ 15.9 hr Sample 3-2 (t₅₀ ~ 16.6 hr Probability (%) 99.5 Sample 3-3 (t₅₀ ~ 17.9 hr Leakage (1E-6 | 100 (E) 1000 1000 10000 100000 10000 100000 Time (second) Time to Failure (second)

Figure 4. Median lifetime (t₅₀) of (A) sample set 1, (C) sample set 2, and (E) sample set 3 and variation in leakage current density with time in (B) sample set 1, (D) sample set 2, and (F) sample set 3.

version once it has been copyedited and typeset. This is the author's peer reviewed, accepted manuscript. However, the online version of record will be diffe PLEASE CITE THIS ARTICLE AS DOI: 10.1063/5.0101308

Figure 5. TSDC data for (A, B) sample 1-1, (C, D) sample 1-2, and (E, F) sample 1-3. For A, C, and E, poling was conducted at 180°C for 4 hours and the TSDC data were measured using a ramp rate of 10°C/min . For B, D, and F, the TSDC measured at ramp gates of 2, 6, 10°C/min after poling at 200 kV/cm at 180°C for 4 hours.





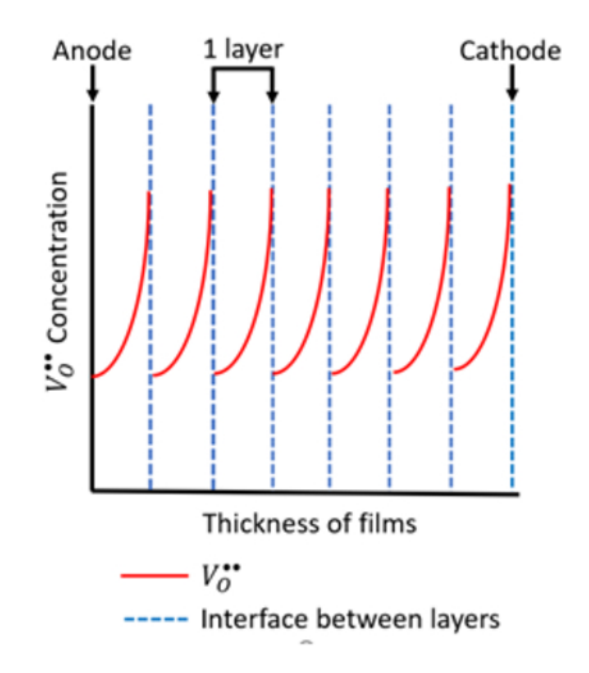


Figure 6. Schematic of gradient in oxygen vacancy concentration in sample 1-2 after poling.